TOPICAL REVIEW • OPEN ACCESS

Optical studies of ferroelectric and ferroelastic domain walls

To cite this article: G F Nataf and M Guennou 2020 *J. Phys.: Condens. Matter* **32** 183001

View the article online for updates and enhancements.

IOP ebooks™

Bringing you innovative digital publishing with leading voices to create your essential collection of books in STEM research.

Start exploring the collection - download the first chapter of every title for free.

Topical Review

Optical studies of ferroelectric and ferroelastic domain walls

G F Nataf[1] and M Guennou[2,3]

[1] Department of Materials Science, University of Cambridge, 27 Charles Babbage Road, Cambridge CB3 0FS, United Kingdom

[2] Department of Physics and Materials Science, University of Luxembourg, 162a avenue de la Faïencerie, 1511 Luxembourg, Luxembourg

[3] Materials Research and Technology department, Luxembourg Institute of Sciences and Technology, 41 rue du Brill, 4422 Belvaux, Luxembourg

E-mail: gn283@cam.ac.uk

CrossMark

Abstract

Recent studies carried out with atomic force microscopy or high-resolution transmission electron microscopy reveal that ferroic domain walls can exhibit different physical properties than the bulk of the domains, such as enhanced conductivity in insulators, or polar properties in non-polar materials. In this review we show that optical techniques, in spite of the diffraction limit, also provide key insights into the structure and physical properties of ferroelectric and ferroelastic domain walls. We give an overview of the uses, specificities and limits of these techniques, and emphasize the properties of the domain walls that they can probe. We then highlight some open questions of the physics of domain walls that could benefit from their use.

Keywords: domain wall, ferroelectric, ferroelastic, optical techniques

(Some figures may appear in colour only in the online journal)

1. Introduction and scope

Ferroic materials are defined by their ability to exist in several possible states, or domains, that can be controlled and switched by an external field. As such, they are functional materials *par excellence*, and have been the object of an intense research activity for decades. Ferroic domains differ only by their orientations and may coexist in the material, where they are then separated by domain walls.

Very often, ferroelectric and ferroelastic domain walls have been considered as mere interfaces, and studied as such. In a classical view, they occupy a negligible volume fraction in the material, and their relevance for physical properties is seen through their motion or their interaction with defects, rather than their specific properties. The idea that ferroelectric and ferroelastic domain walls have their own physical properties has been discussed as early as the 1970s based on theoretical models [1]. Their specific symmetry properties have also been pointed out (e.g. [2]). More recently, following a seminal work in the late 1990s [3], the experimental characterization of specific domain wall properties has enjoyed a renewed interest [4–7], with unusual conductivity in insulators [8–15], or polar properties in non-polar materials [16–25]. These observation, together with the intrinsically small size of the domain walls, often down to a few unit cells only, has led to a new paradigm for devices, named domain wall engineering, where the domain wall rather than the bulk material is the active element [4–7].

Progress in this new field requires experimental techniques able to give insight into the internal structure and specific

properties of domain walls. The very small size of ferroelectric and ferroelastic walls is clearly a challenge. The recent surge in the field has a lot to do with the development of experimental techniques with very good spatial resolution. This includes state-of-the-art atomic force microscopy in its various modes of operation (conductive, piezoelectric force, etc) [8–14], or high-resolution transmission electron microscopy (HRTEM) for atomistic pictures [25–27]. In contrast, experimental techniques that make use of visible light as a probe are often quickly discarded: their spatial resolution is diffraction-limited and comparatively poor. Yet they have been instrumental in historical studies of ferroic transitions and ferroic domains, and there is considerable knowledge on the interaction of light with ferroic materials that can be built upon.

In this review, we provide an overview of the uses of optical techniques for the characterization of the physical and structural properties of ferroelectric and ferroelastic domain walls. We consider as optical techniques methods that use visible light in a broad sense as a probe, and as such are by default diffraction-limited. We emphasize their specificities and limits, with the aim to encourage their use and developments. We show that they are very insightful, not only to image domain walls but also to investigate the structure and physical properties of interest. We then highlight some open questions of the physics of domain walls that could benefit from their use.

Since this is a review about *domain walls*, we do not seek to inventory all papers reporting optical observations of ferroic *domains*. Instead, the focus is on those papers where the structure and properties of the domain walls were explicitly addressed and the experimental data analyzed for that purpose. There is admittedly a grey zone in between, and some degree of arbitrariness in this selection, especially for earlier studies where domain wall engineering was not yet under focus and properties of domain walls treated as a side topic. However, we believe that this review captures the main contributions to the field and will correctly serve its purpose.

This review also does not cover techniques where visible light is used for excitation only, while the imaging itself relies on a different signal. This is the case, for example, for atomic force microscopy measurements under illumination, which have revealed the increase of the electrical conductivity of domain walls under UV light in lithium niobate (LiNbO$_3$) [28, 29], or the enhancement of local photovoltaic and photoconductive properties of domain walls in bismuth ferrite (BiFeO$_3$) thin films [30]. Another example is pyroelectric scanning microscopy [31–42] where pyroelectric currents are mapped in response to a chopped laser-beam focused on an electrode. This technique has been used to study domain structures in several ferroelectrics [32–37], including a report of scans across a domain wall in triglycine sulphate (TGS) [35]. Although these techniques are clearly very relevant to the studies of domain walls, we did not consider they fall into the families of optical techniques.

Finally, this review focuses on ferroelectric and ferroelastic domain walls, and leaves purposely aside magnetic domain walls. This is because the physics of ferromagnetism is very different from ferroelectricity and ferroelasticity, in particular due to the existence of magnetic exchange interactions which have no analog in dielectrics (for a review on magneto-optical microscopy, readers might refer to [43]).

2. Polarized light microscopy

Optical microscopy is a simple non-contact method ideal to observe *in situ* the response of ferroelastic domain walls to temperature [44–48], electric field [48–61] or stress [62, 63]. In transmission, the use of crossed-polarizers, combined with a spatial resolution of the order of a half wavelength of light, produces high-contrast images of the domain structure. The contrast is a direct consequence of the spontaneous birefringence of ferroelastic domains [64, 65]. When visualized with white light illumination, intensity and color variations reveal differences in optical indicatrix with different birefringence magnitudes and extinction directions, which correspond to distinct orientations of domains within the sample. Images are also strongly affected by strain, which can for example arise from defects such as cracks. Optical microscopy thus gives quickly qualitative information about the domain structure. In this section, we give only a brief overview required to understand key concepts of optical imaging (readers might refer to [66–69] for details on optical microscopy studies of ferroic domains).

At the state-of-the-art, the polarization dependence under monochromatic light is used to quantify birefringence differences, and measure separately (i) the transmitted intensity, (ii) the orientation of the indicatrix and (iii) a function of optical retardation for light travelling in that direction described as $|\sin\delta|$ where $\delta = (2\pi/\lambda)\Delta nL$ with λ the wavelength, L the sample thickness and Δn the birefringence [70].

As an early example of such work, figure 1 shows ferroelastic domains in Ameralik anorthosite. The color map reveals yellow, red and purple zones corresponding to $|\sin\delta|$ values between 0.4 and 0.6. Interestingly, domain walls appear as green lines with $|\sin\delta| = 0.3$. This contrast is tentatively attributed to strain although the authors could not conclusively rule out a spurious effect caused by tilting of domain walls [70].

Indeed, the diffraction-limited resolution and the small divergence of the transmitted light, combined with the spontaneous birefringence of ferroelastic domains and small inclinations of domain walls can easily cause misleading interpretations. In particular, size of domain walls optically observed are unrealistically large: 0.4 μm in barium titanate (BaTiO$_3$) [60], 3–5 μm in lead germanate (Pb$_5$Ge$_3$O$_{11}$) [46] and gadolinium molybdate (Gd$_2$(MoO$_4$)$_3$) [71].

An original optical way to visualize the consequences of the inclination of the domain walls with respect to the direction of propagation of the incident light is to observe interferences created by the interaction of primary and secondary monochromatic beams, as documented in [45, 72–74].

Optical observations, and the precise understanding of the domain structure they permit, can also be used to identify physical properties of domain walls without probing them
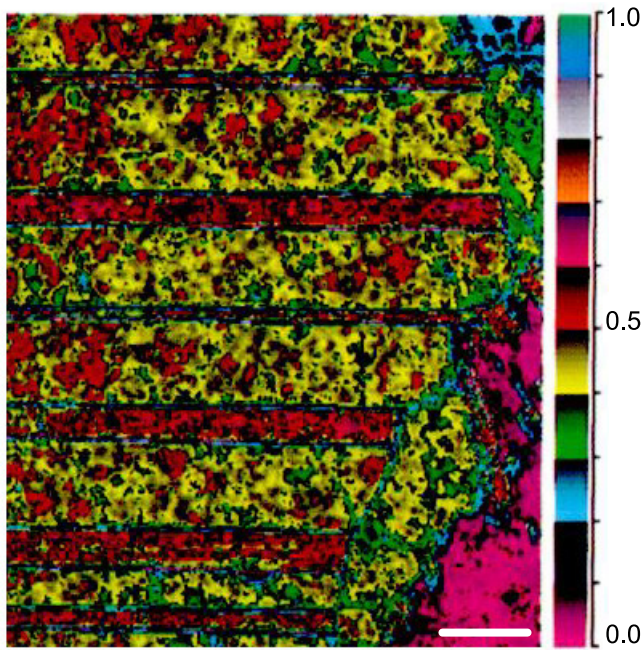
Figure 1. Optical microscopy on ferroelastic domain walls. |sinδ|, retardation image of a section of Ameralik anorthosite (thickness 0.03 mm). The horizontal scale bar is 0.1 mm. Reproduced with permission from [70].
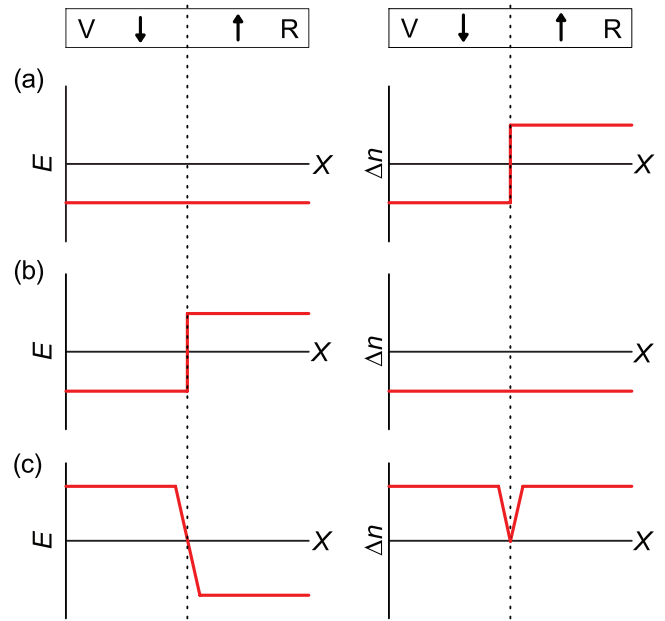

Figure 2. Sketches illustrating the mechanisms leading to a contrast observable in optical microscopy at 180° ferroelectric domain walls. A schematic of electric fields along the polar axis of Z-cut LiTaO$_3$ crystals and the corresponding change in ordinary refractive index Δn in the c plane through the electro-optic effect across a domain wall. (a) Crystal at room temperature, (b) crystal after annealing at 350 °C for 12 h, and (c) crystal after creating pyroelectric fields on the surface. The dashed vertical line indicates the domain wall. 'R' and 'V' stand for reversed and virgin, respectively. Reprinted from [82], with the permission of AIP Publishing.

directly. For example, in tetragonal BaTiO$_3$, charged domain walls observed in transmission appear as bright or dark lines on the $(1\,1\,1)_{pc}$ surface, with respect to the pseudo-cubic axes, as a result of the different orientations of adjacent domains [75]. Combined with the knowledge of the direction of the electric field applied to create this domain structure, it allows the assignment of bright and dark lines to positively and negatively charged domain walls, respectively.

In the case of non-ferroelastic domain walls, there is no difference in birefringence between 180° domains. As a result, unless the ferroelectric polarization is accompanied by optical activity (as in Pb$_5$Ge$_3$O$_{11}$ [76]), domains will appear identical in transmission microscopy (as in the important uniaxial ferroelectrics LiNbO$_3$ and LiTaO$_3$). This situation is beneficial for the study of domain walls, which will stand out against a uniform background, but obviously a problem when seeking to distinguish domains of different orientations. A large amount of work was therefore invested to create some contrast between the domains. This is possible with an external electric field. This technique, called electro-optic imaging microscopy, takes advantage of the linear electro-optic effect to induce refractive-index changes in the domains by applying an electric field and thus generates birefringence contrast at the domain wall [37, 48–50, 77–81]. For example, in uniaxial ferroelectrics such as LiNbO$_3$, an external electric field applied in the same direction as the ferroelectric polarization decreases the value of the ordinary refractive index while it increases its value if the electric field is applied in the opposite direction, and leads to different refractive indices in adjacent domains [50, 79]. In BaTiO$_3$, a field orthogonal to the domain walls gives similar contrasts [49].

In the case of 180° domains in BaTiO$_3$, the contrast between domains has been observed to persist for a short period of time after removal of the electric field (or the formation of the domains) [51–57], with the reversed domains generally appearing darker than the virgin domains.

In lithium tantalate (LiTaO$_3$) and LiNbO$_3$, even in the absence of applied electric field [78, 82, 83], the contrast at domain walls persists (without evidence of relaxation), but vanishes after thermal annealing [82]. Indeed, in an unannealed sample of LiNbO$_3$ or LiTaO$_3$, where domain reversal was performed at room temperature, intrinsic polar defects induce an internal electric field [82] which leads to a change in ordinary index across domain walls, as schematized in figure 2(a). For an internal electric field $E_{int} = 5.5$ kV mm^{-1}, and an electro-optic coefficient $r_{13} = 8.4$ pm V^{-1} the expected change in refractive index across the domain wall is $\Delta n = 4.5 \times 10^{-4}$.

Upon annealing, polar defects reorganize, the internal field in the domain-reversed regions (R) realigns with the main polarization direction induced during poling at room temperature, as shown in figure 2(b), and leads to the loss of optical contrast at domain walls.

The contrast is recovered if the sample is heated up or cooled down rapidly, since fast changes in temperature create pyroelectric charges. This effect, sometimes coined pyroelectrooptic effect, has been invoked in a number of studies on ferroelectric domain walls [78, 84–86]: charges of opposite signs accumulate in adjacent domains of opposite polarizations and compensate each other across the domain wall, which results

in a local field distribution equal to zero, as shown in figure 2(c). This provides a decrease of the refractive index close to the domain walls, and generate the observed contrast [82].

Polarized light microscopy is not the only optical way to visualize changes in refractive indices. They can be probed by electro-optic scanning microscopy, which relies on the detection of intensity variations of a monochromatic light reflected on the sample. Under an AC electric field, this gives rise to a black and white contrast between 180° domains [87, 88]. With lock-in amplification, this method appears more sensitive and operate at smaller fields than polarized light microscopy [87, 88]. Changes in refractive indices can also be calculated from diffraction patterns resulting from the scattering of monochromatic light by domain walls in optical Bragg geometry, as successfully performed in $LiNbO_3$ (under DC electric field) [89–91].

A few studies of ferroelastic domain walls have been performed in reflected light instead of transmitted light. In the case of $YBa_2Cu_3O_{7-x}$ with a high density of domain walls (domain size below 5 nm), complex contrasts observed as a function of the positions of the polarizers have been attributed to a possible slight difference in refractive index between domain walls and domains [47].

3. Optical coherence tomography

Optical coherence tomography is based on a Michelson interferometer, where a laser is fed into a reference arm and the sample is illuminated through a microscope objective [92]. Back-reflections of the light by sub-surface features, where the optical indicatrix changes (e.g. domain walls), are collected by the same objective and superposed with the reference signal on a detector. The obtained interference pattern is characterized by spectral oscillations from which it is possible to reconstruct the spatial (axial) position of the features through fast Fourier transformation. The main advantage of this technique is that it can operate in the MHz region and provide fast 3D-images of domain walls over several hundreds of micrometers [93].

Optical coherence tomography has been used to profile the refractive-index across 180° domain walls in $LiNbO_3$ [93–95]. For ordinary polarized incident light no signal is recorded, while for extraordinary polarized light, domain walls appear as planes (figure 3(b)) whose positions match with boundaries of the domains as seen by optical microscopy on the surface etched after the measurement (figure 3(a)). The contrast obtained is equivalent to a difference in the extraordinary index of 4.2×10^{-4} [94]. If this contrast resulted from the internal electric field, it should have the value 1.0×10^{-4} (with $E_{int} = 3$ kV mm^{-1} [96], $r_{33} = 34$ pm V^{-1} [97] and $n_e = 2.2$ [98]). Furthermore, the contrast remains constant under an applied electric field, ruling out the electro-optic effect as the main mechanism [93]. These results suggest that the refractive index profile across domain walls exhibits a complicated shape, which could for example be realized by field independent kinks localized at domain walls. Similar measurements have been performed on near-stoichiometric
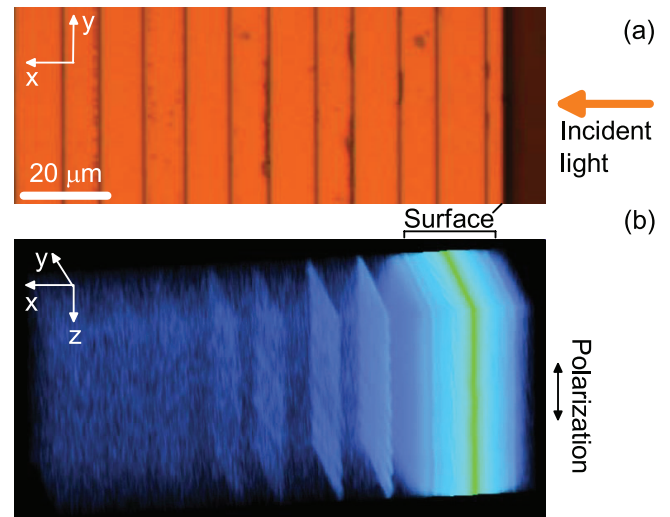

Figure 3. Optical coherence tomography. (a) Optical image of an etched surface of a $LiNbO_3$ single crystal revealing domain walls (black lines). The orange arrow indicates the direction of the incident light. (b) 3D color-coded representation of the axial scan signal on an un-etched sample. Reproduced from [94]. CC BY 4.0.

$LiTaO_3$ [94]. However, the spectral oscillations are found to be much smaller than in congruent and magnesium-doped $LiNbO_3$, indicating that defects and internal fields play a role in the observed contrast.

It is important to keep in mind that optical coherence tomography relies on back-scattered light, with an acceptance angle of a couple of degrees only. Therefore, strongly inclined domain walls will not be visible [95]. Also, kinks in the domain walls (as small as 50 nm) can lead to destructive interference of the back-scattered light and decrease the amplitude of the signal [95]. Thus, a lack of signal does not prove the absence of domain wall.

4. Second harmonic generation

Second harmonic generation (SHG) is a nonlinear optical process in which two photons with the same frequency interact with the medium, and generate a new photon with twice the frequency of the initial photons [99]. SHG microscopy produces images where the contrast originates from variations of the non-linear optical susceptibility. Because this susceptibility is described by a 3rd-rank tensor, a centrosymmetric material is inherently non SHG active by symmetry. This is the case for example of ferroelastics calcium titanate ($CaTiO_3$), lead phosphate ($Pb_3(PO_4)_2$) and lanthanum aluminum oxide ($LaAlO_3$). However, three-dimensional observations of these materials with SHG reveal that while domains are indeed non SHG active, domain walls exhibit SHG activity. The interpretation of these findings is that centrosymmetry is broken at the domain walls, i.e. that the domain walls are polar [20–23].

SHG can be used to determine the direction of the polarization vector of the domain walls, through polar diagrams. The principle is to record the SHG intensity for different directions of the polarization of the incident light; the polarization of the

second harmonic signal being kept parallel to it. For a 360° rotation of the polarization, domain walls exhibit a double-wing diagram with a twofold symmetry, which once fitted gives the symmetry of the domain walls and the direction of the polar axis with respect to the domain wall plane [20–23]. To date, SHG is the only experimental technique which has been able to determine the symmetry of domain walls, and therefore allows comparisons with theory. It has also been instrumental in the recent searches for 'Bloch-like' and 'Néel-like' ferroelectric domain walls, i.e. symmetry breaking in the polarization profiles across the domain walls [100].

In $CaTiO_3$, the symmetry is found to be m when investigating domain walls both in as-grown crystals [20] and induced by uniaxial stress [21]. It has also been reported that the polarization can lie out of the domain wall plane when there is another domain wall in the vicinity (about 20 μm away), suggesting an interaction between domain walls. The same m symmetry is obtained for $Pb_3(PO_4)_2$ [23]. In $LaAlO_3$, the best fit is obtained with a $3m$ domain wall symmetry [22].

The observation of ferroelectric domain walls is *a priori* more difficult because ferroelectric domains themselves exhibit a strong SHG signal. Still, domains and domain walls were observed in $BaTiO_3$, potassium titanyl phosphate ($KTiOPO_4$), $LiNbO_3$ and $LiTaO_3$ by SHG in a backscattering geometry [101–103]. In these works, domain walls appear as dark lines, i.e. show no SHG signal, which correspond to the expectation from a simple volume average when crossing a canonical ferroelectric Ising domain wall, where the amplitude of the polarization gradually decreases down to zero before reversal [102–105].

Other studies have reported a *bright* contrast, i.e. an enhancement of the SHG signal, with experiments in transmission geometry [107–110], or in the so-called Čerenkov SHG, where the SHG is emitted at an angle with respect to the propagation direction of the incident light [111–114]. The origin of this enhancement has been discussed in several instances with a number of effects: local electric field, defects partially depolarizing and imposing interface selection rules, interference of the second harmonic waves generated by different parts of the incident light that covers simultaneously adjacent domains, presence of kinks and complex refractive-index profiles at domain walls [27, 108–112].

In transmission geometry it is also possible to set the incident light at an angle with respect to the ferroelectric axis, such that domains are in phase-matching conditions (i.e. with constructive interference). Domain walls appear then as dark lines as a consequence of destructive interference from optical rays originating from adjacent domains. If the crystal is moved away from the phase-matching direction such that there is now destructive interference in the domains but not in the vicinity of the domain wall, domain walls appear bright on a dark background [115].

It is possible to obtain detailed images of domain walls with SHG, e.g. of the roughness of head-to-head domain walls in $LiNbO_3$ [112, 113], but it takes careful polarization analysis to associate conclusively the observed signal to an internal structure of the domain wall [106]. In $LiNbO_3$, the second-order
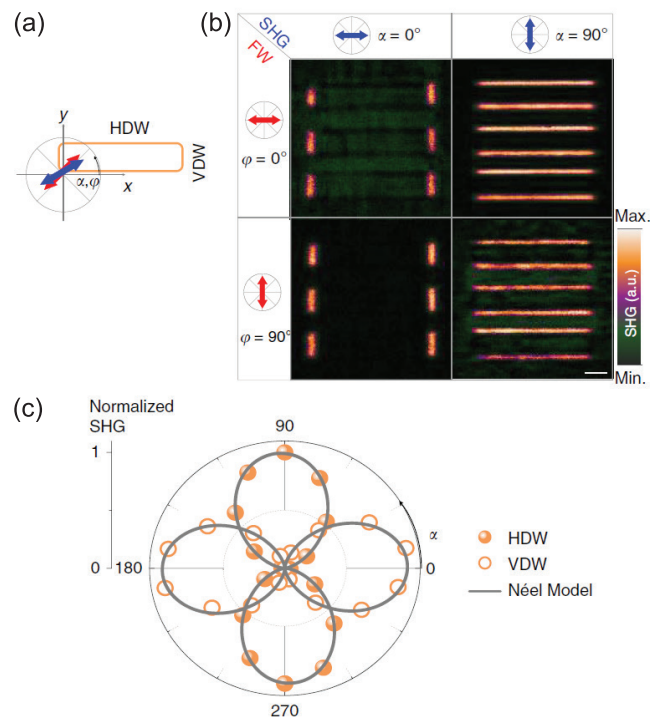

Figure 4. Second harmonic generation in tetragonal $Pb(Zr,Ti)O_3$. A systematic analysis of the local SHG is conducted for different polarizer and analyzer settings, at horizontal (HDW) and vertical (VDW) domain walls, as schematically illustrated in (a). (b) SHG measurements conducted in rectangular-shape c-domains exhibit maximum signal at HDWs and VDWs when the analyzer (blue arrow) is perpendicular to the domain walls. (c) Corresponding polar plots (scattered dots) of the normalized SHG intensity measured at a fundamental polarization angle $\varphi = 0°$. The continuous lines are fits of the experimental data to the analytic expression of the SHG intensity expected for Néel-type walls with horizontal and vertical orientations. Reproduced from [106]. CC BY 4.0.

susceptibility tensor of domain walls has been obtained by SHG and compared with the bulk tensor of the domains. The comparison reveals that the mirror inversion symmetry is violated and the threefold rotational symmetry is retained, indicating a symmetry reduction at the domain wall [116]. In $LiTaO_3$ it shows Bloch-like configurations at domain walls [106].

Through a similar approach the polarization profile across 180° domain walls in lead zirconate titanate ($Pb(Zr,Ti)O_3$) has been probed [106]. Figure 4(b) shows SHG images measured in parallel or crossed-polarization for domain walls schematized in figure 4(a). The fitting of the polar diagram obtained in figure 4(c) reveals the existence of a planar polarization within the domain walls, with Néel-like configurations, instead of the ideal Ising configuration that is traditionally expected [106].

5. Micro-Raman spectroscopy

Micro-Raman spectroscopy relies upon inelastic scattering of light, known as Raman scattering. A laser beam is focused on a sample where it interacts with matter and is scattered inelastically with some energy shift that corresponds to interactions

with excitations in the medium, most typically phonons or magnetic excitations [117].

Two measurement strategies can be adopted to study ferroelectric and ferroelastic domain walls with micro-Raman spectroscopy. It is possible to investigate a single domain wall by performing a line-scan and comparing spectra acquired far from the domain wall and on the domain wall [118–127]. Or, a spectrum acquired on an area with a high density of domain walls can be compared with a spectrum acquired on a wall free area [128, 129]. In both cases, the influence of domain walls appears as changes of intensity, frequency and width of the Raman peaks or as the emergence of new peaks. Interpreting these subtle variations is not an easy task and it is the purpose of this section to propose an overview of the changes reported in the literature and their interpretations.

Because of the large size of the laser spot compared to the domain wall thickness, the Raman signal at the interface between two domains contains a weighted average of the different Raman signals from both domains, and a possible extra signature from the domain wall. Just like in optical microscopy, 180° non-ferroelastic domains have identical Raman signals and the contribution of the domain walls stands out easily. On the other hand, ferroelastic domains will in general exhibit a contrast due to their different orientations, which complicates the extraction of the specific domain wall signature.

In LiNbO$_3$, line-scans reveal intensity maxima of transverse E modes (E(TO1) and E(TO8)), and intensity minima of longitudinal mode A$_1$(LO4) in the vicinity of 180° domain walls [121–124]. These intensity variations could be induced by a local strain field—or a local electric field since both are coupled through the piezoelectric effect.

While this local electric field could be an intrinsic characteristic of the domain wall, it has been argued that it could also arise from an experimental artifact: the Raman laser could heat-up the domain wall, causing uneven charging through the pyroelectric effect, and creating *in fine* a local electric field [119].

The same explanation could hold for intensity increases on the shoulders of Raman peaks [125] since a local electric field could lead to depolarization of incident and backscattered light, breaking symmetry rules and allowing forbidden Raman peaks.

To identify and isolate Raman changes induced by defects segregated at domain walls, it is common to investigate samples with different amounts of defects. For example, frequency shifts reported at domain walls are larger in congruent LiNbO$_3$ than in near-stoichiometric LiNbO$_3$ [118–120]. Since the defect density (niobium antisites and lithium vacancies) is higher in congruent LiNbO$_3$, it indicates that these shifts are influenced by defects localized at domain walls.

It is also possible to intentionally introduce defects (dopants) in a sample. This strategy has been successful to understand the origin of frequency shifts observed at domain walls in LiNbO$_3$ [126]. As shown in figure 5, line-scans across domain walls reveal a frequency shift of the Raman modes between domains, which do not change monotonously with doping. In 1%, 2% and 3% magnesium-doped lithium niobate the frequency of all modes is slightly higher in reversed
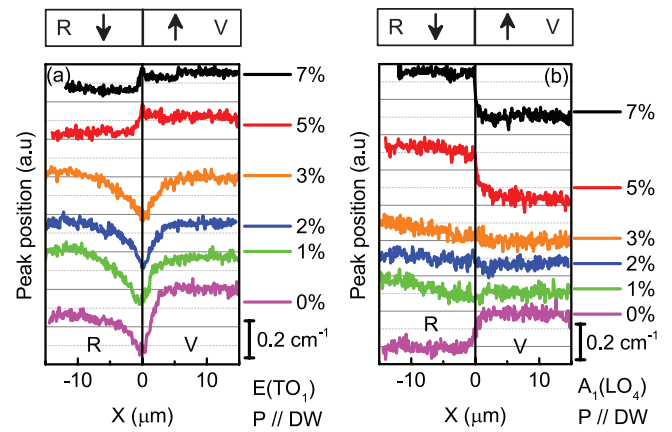

Figure 5. Micro-Raman spectroscopy on ferroelectric domain walls in magnesium-doped LiNbO$_3$. Peak position of (a) E(TO1) and (b) A$_1$(LO4) for line-scan from reversed (R) to virgin (V) domains for different amounts of magnesium before annealing. The data are vertically shifted for clarity and the scale bar gives the amplitude of the frequency shift. [126] John Wiley & Sons. © 2016 WILEY-VCH Verlag GmbH & Co. KGaA, Weinheim.

domains. On the other hand, in 5% and 7% magnesium-doped lithium niobate, the frequency of E(TO1) is decreased while the frequency of A$_1$(LO4) is increased in reversed domains. After annealing at 200 °C, the contrast between domain vanishes, pointing out polar defects and the resulting internal electric field as its origin [82]. The contrast at domain walls persists, and as such indicates a stabilization of defects at domain walls. However, the contrast differs from the signature of polar defects previously described. This observation indicates that, in addition to the influence of defects previously reported, local electric field variations should also be taken into account in order to interpret frequency shifts at domain walls [126].

In ferroelastic materials, the analysis is more challenging since, as explained previously, ferroelastic domains exhibit different intensity ratios between Raman peaks. This is the main reason why only a few ferroelastic domain walls have been investigated with micro-Raman spectroscopy [71, 128–130]. In lead phosphate-arsenate (Pb$_3$(P$_{1-x}$As$_x$O$_4$)$_2$), a Raman spectrum acquired on an area with a high density of domain walls (about 80 domain walls within the laser spot), compared with a spectrum acquired on an area free of domain walls, reveals a low-frequency shoulder on the peak at 541 cm^{-1} and an extra peak at about 65 cm^{-1}. The emergence of new peaks is an indication of structural rearrangements at the domain wall [128, 129].

In Gd$_2$(MoO$_4$)$_3$, a phase-sensitive lock-in amplifier has been used to synchronize the Raman measurement with the movement of a single ferroelastic domain wall induced by an AC electric field. The spectrum obtained exhibits enhanced intensity where Raman peaks from the high-temperature tetragonal phase are expected, which suggests that the domain wall has a structure close to the tetragonal high-temperature phase [71], in agreement with the theoretical expectations.

Micro-Raman spectroscopy has also been used to perform depth scan profiles across domain walls in BaTiO$_3$. It has been argued that by changing the polarization direction of the
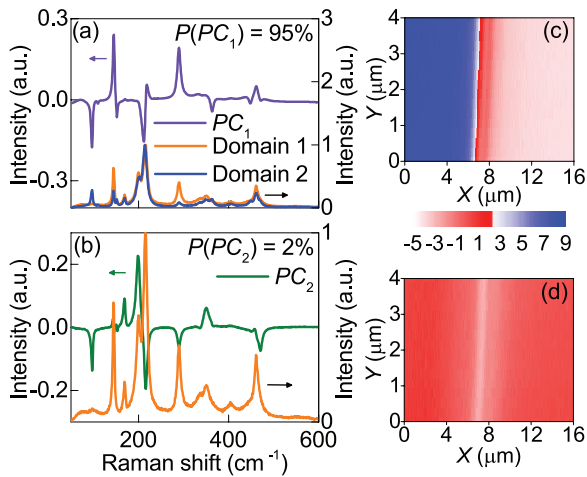
Figure 6. Principal component analysis (PCA) of Raman maps of ferroelastic domains and domain walls in NdGaO$_3$. (a) Comparison of PC1 and two spectra from domain 1 and domain 2. (b) Comparison of PC2 with a spectrum from domain 1. (c) Scores of PC1 for every spectrum. (d) Scores of PC2 for every spectrum. Reproduced from [127]. © IOP Publishing Ltd. All rights reserved.

Figure 7. Photoluminescence microscopy. Spectral position of the emission for a scan across a domain wall (see inset) in a nearly stoichiometric Er-doped LiNbO$_3$ single crystal before and after annealing (5 h, 250 °C). Reprinted from [134], Copyright 2007, with permission from Elsevier.

incident laser, it is possible to move ferroelectric domain walls [130]. This hypothesis will require further confirmation, notably in order to exclude birefringence effects that are known to affect Raman depth profiles and, consequently, distort images constructed from Raman 3D maps [131, 132].

Progress in the field of Raman spectroscopy on ferroelectric and ferroelastic domain walls might arise from the development of multivariate statistical methods (e.g. principal component analysis—PCA) to analyze the data [127]. Applied to Raman maps, these methods can identify correlated changes in the Raman signal at the location of the domain wall. As shown in figure 6, PCA on spectra acquired across a ferroelastic domain wall in neodymium gallium oxide (NdGaO$_3$) reveals two components (figures 6(a) and (b)), such that subtracting the first component (PC1) from a spectrum of domain 1 gives a spectrum characteristic of domain 2. Thus, PC1 describes the domain structure and the weighted average of the Raman signal from both ferroelastic domains at the domain wall. PC2 must then describe an extra contribution observed in the vicinity of the domain wall. This conclusion is consistent with the fact that the score of PC1 reveals the two domains (figure 6(c)) while the score of PC2 is located at the known position of the domain wall (figure 6(d)). Therefore, PCA can be used to separate the contribution of ferroelastic domains and domain walls, and in the case of NdGaO$_3$ evidence intensity variations that still have to be interpreted [127].

In summary, micro-Raman spectroscopy has the advantage of probing strain fields, electric fields and defects at domain walls. While distinctive signature are very often seen at domain walls, their analysis and significance has yet to be understood, certainly with the support of theoretical modelling.

6. Photoluminescence microscopy

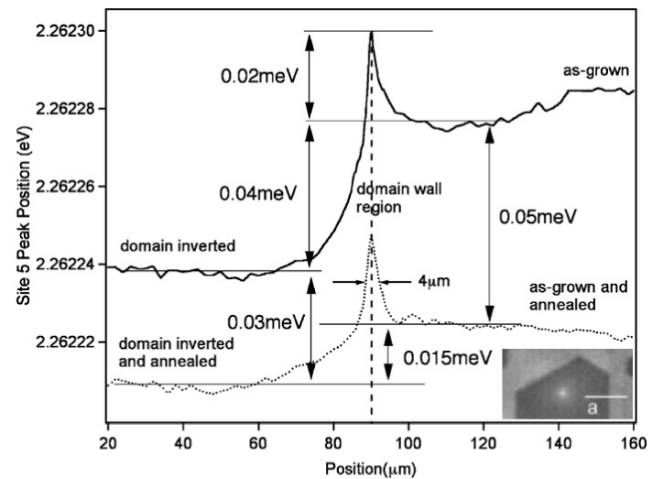Photoluminescence is light emission from a material resulting from a radiative de-excitation of electrons previously excited to higher energy levels by absorption of an incoming light [133]. Photoluminescence studies can be done either by using an excitation light above the band-gap of the material itself or—more commonly—by incorporating in the crystal of interest some photoluminescent dopant and use its signal as a probe for its structural environment.

Photoluminescence microscopy has been used on LiNbO$_3$ intentionally doped with a small amount (10^{-1} mol%) of Er^{3+} cations [134–137]. Er has been chosen because it has been the topic of extensive investigations over the years for application as active ions in solid-state lasers [138]. Er^{3+} occupies the Li$^+$ site, but different charge compensation mechanisms lead to 11 different configurations of the Er^{3+} defect sites. The integrated emission intensities indicate the relative abundance of the sites. A direct comparison of the spectra obtained after electric field poling (which leads to a rearrangement of Er^{3+} ions) or after annealing (at temperatures where defects are mobile) gives insights into the influence of defect rearrangements or local electric field variations on the photoluminescence signal [134].

This knowledge can then be used to understand changes observed in the vicinity of 180° domain walls (figure 7). For example, line-scans reveal that the peak position of the defect site labeled A1 varies, indicating a change in the electric field that is experienced by the Er ion probe [134]. The contrast between domains is affected by annealing, suggesting that it arises from polar defects and the resulting internal electric field [96]. On the contrary, the contrast in the vicinity of the domain wall persists after annealing. The shift in spectral position indicates a change in electric field of 60 kV cm^{-1}. However, it might not be the indication of misaligned defect dipoles at the domain wall but rather simply a consequence of the different positions of Nb and Li ions on either sides of the domain wall, due to the opposite electric polarizations of the domains. This may indeed lead to a difference in the position of the Er ion away from the value determined in the bulk material [134].

It is also possible to take advantage of dopants already used commercially for LiNbO$_3$, e.g. magnesium which reduces

optical damage upon high power laser irradiation. Multi-photon laser scanning luminescence microscopy measurements in 5% magnesium-doped LiNbO$_3$ reveal a clear contrast at domain walls [139], tentatively attributed to higher dopant concentrations [139], based on the fact that, in this regime, the luminescence intensity scales with magnesium concentration [140, 141]. However, internal field variations and local changes in strain could also play a role [140, 141].

Photoluminescence microscopy applied to domain walls has received relatively little attention, in spite of its sensitivity to the local environment of the dopants, and thereby its potential to unveil details of the electric or strain fields at domain walls. This might be because, just like for micro-Raman spectroscopy, the interpretation of the observed signals may not be straightforward, and may require a deep knowledge of the dopant behavior in the bulk, as well as comprehensive theoretical work.

7. Super-resolved techniques

Microscopy techniques are called super-resolved when they are able to overcome the diffraction limit, which can be done notably by working in the near-field regime. They are of course very appealing for the studies of domain walls, but can be very challenging both in their implementation and interpretation [142–158].

Near-field scanning optical microscopy (NSOM, or SNOM) has been used to image domain structures in several ferroelectrics [142–154], with contrast observed at domain walls in LiTaO$_3$ [142, 150, 151], LiNbO$_3$ [147, 148], TGS [143, 153], BaTiO$_3$ [144] and Ba$_2$NaNb$_5$O$_{15}$ [147]. These measurements have been performed in different modes of operation. In the illumination mode, the sample is illuminated with a fiber maintained a few nanometers above the surface and the light collected in transmission by an objective [142–147]. In the collection mode (CNSOM), polarized light is transmitted through the sample under study and collected with a fiber maintained a few nanometers above the surface [146, 148, 150, 151]. The same fiber can also be used both for illumination and collection [143]. Finally, in the reflection mode, the sample is still illuminated with a fiber but the light is collected in reflection by an objective [146, 147, 153]. The small aperture of the fiber (typically a hundred of nanometers) and the use of a metal coating to force the light to enter the aperture, allows spatial resolutions better than a fifth of a wavelength of light [146, 148–150, 152].

Most studies remain qualitative in their description of the index variations in the vicinity of the domain walls, but there are examples where the authors quantify the effect. For example, in LiNbO$_3$, in the vicinity of the domain wall, complex changes of intensity are observed with CNSOM and compared with simulations of the intensity profiles obtained through the beam propagation method, in order to determine a refractive index profile, as shown in figure 8. A change in refractive index of $\Delta n = 1 \times 10^{-3}$ extending over 20 μm is found and attributed to the internal electric field [148]. An additional sharp index profile kink of the same order of magnitude but extending over
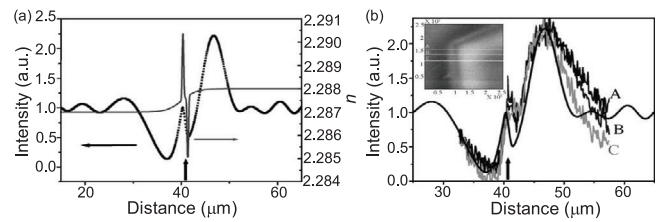

Figure 8. Collection mode near-field scanning optical microscopy (CNSOM). (a) Simulated refractive index profile and intensity of light emerging after propagation through a domain wall in a 500 μm thick crystal of LiNbO$_3$. (b) Comparison of the experimental and modeling profiles of the intensity variations. Reprinted from [148], Copyright 2005, with permission from Elsevier.

only 2 μm remains unexplained [148]. In reflection mode, $\Delta n = 10^{-4}$ extending over 30 μm is found [147].

Also, in LiTaO$_3$, a change in refractive index $\Delta n = 5 \times 10^{-5}$, corresponding to an internal electric field of ± 10 kV mm^{-1}, extends on only 200 nm to 1 μm [142, 150, 151]. Under an *in situ* electric field, the observed optical signal reveals birefringence variations with a spatial resolution of about 100 nm. Application of an external electric field reveals the pinning of domain walls by subsurface defects, which are evidenced by an increase in birefringence and bowing of the domain wall [151].

One of the main challenges for the interpretation of NSOM images in collection and illumination modes is a direct consequence of the spatial extension of domain walls that are crossing the whole sample thickness. Close to the surface, domain walls are in near-field conditions but deeper in the sample they are in far-field conditions and lead to usual diffraction-limited patterns, decreasing the overall spatial resolution of the image obtained [144]. Furthermore, the secondary light rays resulting from the interaction with domain walls in the far-field region have different phases and combine with the light emitted at the surface. This might be the reason for the large spatial extension of features observed at domain walls with these modes [142–144, 147, 148, 150, 151]. On top of that, small differences in refractive index between domains make them act as waveguides with light confined in the high refractive index regions and as a consequence concentrated at certain spots [147, 149, 159, 160].

In a similar spirit, over the past 20 years, there has been a sustained effort to push optical spectroscopy techniques (infrared, Raman, photoluminescence) beyond the diffraction limit. Tip-enhanced Raman spectroscopy (TERS) takes advantage of the enhancement of Raman scattering at the apex of a near atomically sharp tip [155–158] to reach spatial resolutions of the order of 15 nm. However, since early achievements on LiNbO$_3$ [156], and BaTiO$_3$ nanocrystals [157], the technique has seen progress rather in the field of molecular spectroscopy or analytical chemistry, and applications to inorganic materials are still scarce [158]. One reason might be that scanning tunneling microscopy-based TERS measurements are challenging on insulating ferroics. The most relevant measurement to date is the TERS enhancement of the Raman signal in double perovskites La$_2$CoMnO$_6$ thin films, even though the experiment does not take advantage of the

improved spatial resolution [161]. For short, while TERS is promising to selectively enhance the signal at the domain wall with respect to the (far-field) signal of the domains, it still requires more technical developments to allow for detailed characterizations. Along the same line, we note that progress are currently being made in near-field infrared and THz spectroscopy, with a recent application to the domain walls in the improper ferroelectric $Ca_3Ti_2O_7$, where a spatial resolution of ~ 20 nm was demonstrated [162].

8. Conclusions and perspectives

From this overview, it is quite clear that optical techniques in general can rather easily *image* domain walls in ferroic materials, in spite of their small size. The challenge is usually to understand the observed contrasts, and relate them to the specific properties of the domain walls—especially in earlier works where the exotic character of domain walls was not yet under scrutiny. We believe that there is room for improvement there, and therefore a significant potential to contribute further to domain wall engineering studies. As an illustration, we describe below some current topics that could benefit from further studies by optical methods.

8.1. Domain wall symmetry and polarization

Symmetry determines physical properties, and domain walls are no exception to the rule. There has been a considerable amount of work to derive the symmetries of domain walls and domain structures [69, 163]. A remarkable and now well established result is that all compatible ferroelastic domain walls are polar [163]. For example, recent calculations show that domain walls in halide perovskites [164] carry a substantial polarization, which could play a role in the photo-ferroelectric effect. There are nonetheless a number of open questions on domain wall polarization and symmetry.

On the theoretical side, the classical derivation of domain wall symmetry is done by selecting the possible layer groups considering (i) a symmetry descent at the phase transition and (ii) the spatial arrangement of domain pairs in real space [163]. An alternative approach, based on the calculation of symmetries in the order-parameter space, has also been proposed to directly couple the layer group symmetry of the domain wall to Landau theory [165, 166].

On the experimental side, measuring the full domain wall symmetry is not a trivial task. As typical examples, many experiments demonstrating the polar character of domain walls in non-polar materials (as in strontium titanate [17, 18], $CaTiO_3$ [24, 25]) give evidence for a loss of inversion symmetry, but cannot be more specific. Optical techniques have an advantage in that it is possible to play on the light polarization and propagation directions. Besides, they can probe the domain wall as a 3D object, i.e. in the bulk, as opposed to local probe techniques that are surface sensitive only. In fact, SHG is so far the only experimental technique that has produced propositions for the domain walls symmetries [20–23].

It has also given evidence [106] for the often predicted non-Ising character of ferroelectric domain walls [167–174]. Other experimental evidences, TEM-based, remain scarce [175, 176].

Yet, SHG also leaves a number of questions, and has produced results that are not consistent with the theoretical predictions. In $CaTiO_3$, no compatible domain wall is predicted to have out-of-plane polarization as observed in [20], and the mechanism behind the proposed interactions between domain walls is not yet clear. Similarly, the domain walls with $3m$ symmetry in $LaAlO_3$ [22] are not predicted by classical approaches [69, 163, 165]. In ferroelectric domain walls, it is not obvious how to reconcile the macroscopic picture and symmetry given by SHG with the microscopic pictures revealed by TEM where the walls are found to consist of kinks and meanders, far from the ideal plane [27].

In principle, Raman spectroscopy is also an option to determine the domain wall symmetry, by conducting a series of polarized measurements. There is no such report yet, but also no fundamental obstacle to do so. The Raman effect, described by a 2nd-rank tensor, can be expected to be complementary to the SHG, described by a 3rd-rank tensor with different selection rules.

An important question related to symmetry is the question of the polar properties of compatible ferroelastic domain walls. While the loss of inversion symmetry is now well established, the observation of a polarization raises the question of a possible ferroelectric, and not only polar, character of domain walls. Indeed, the ability to switch polarization in the domain wall is critical for applications. Ultimately, the proof for this will have to be a measurement of the dielectric properties of the wall. Nonetheless, we note that SHG and micro-Raman spectroscopy are both compatible with *in situ* measurements under electric field or stress, and could be very useful in the characterization of domain walls under field.

8.2. Domain walls as phonon filters

Controlling thermal fluxes as easily as electric and electromagnetic fluxes requires manipulating the motion of phonons, which have no mass and no bare charge and are therefore difficult to control with an external field.

Several calculations indicate that ferroelectric and ferroelastic domain walls have a large effect on phonon transport, and hence heat flux [177–181]. For example, a single domain wall in lead titanate increases by up to 20% the thermal resistance of a bulk sample [180]. It is also reported that 180° domain walls have different influence depending on the polarization of the phonons: domain walls suppress most of the transverse modes while they are typically transparent for the longitudinal ones [181]. Since ferroelectric and ferroelastic domain walls can be written and erased at wish through the application of an electric or stress field, they could be used to control heat fluxes [178].

A couple of measurements of the thermal conductivity of single domain and multi-domain single crystals confirm the

influence of domain walls on thermal conductivity and the ability to control the thermal conductivity by applying an external field [182, 183]. However, they consist only of bulk measurements.

Micro-Raman spectroscopy could be used to probe phonons near domain walls and give the first local insight into the phonon scattering predicted at domain walls. Investigating several materials at different temperatures, and different domain walls geometries (head-to-head, tail-to-tail) would provide experimental values to compare with calculations.

Infrared camera measurements, which now easily reach thermal resolutions of 20 mK and spatial resolution of 6.5 μm [184], would be good complementary measurements which would provide insights into temperature changes around domain walls.

8.3. Local photovoltaic effect and photoreactions

The anomalous photovoltaic effect in $BiFeO_3$ thin films with a high density of domain walls, which results in open circuit voltages larger than the band gap of $BiFeO_3$, attracted a lot of interest [185]. The effect has been first suggested to arise from the local electric field, which separates electron-hole pairs at domain walls and modifies locally the electrostatic potential [185]. But it has then been shown that the bulk photovoltaic effect in itself, when taking into account the enhanced conductivity at domain walls, can also explain the anomalous photovoltaic effect [186].

Photoluminescence microscopy measurements could be used to probe the local band structure of such films in order to account for possible changes of the electrostatic potential in the vicinity of domain walls. Measurements could be performed as a function of temperature or under a secondary illumination to correlate results of the photovoltaic effect with changes of the band structure.

Another elegant way to investigate changes in the electronic band structure at the domain wall would be to take advantage of resonant Raman signatures and perform line-scans with different excitation wavelengths [187].

Photoreactions, such as photocatalysis or photochemical reductions/oxidations, are also a hot topic in the field of photoferroelectrics. The ability to control the location of the reactions by taking advantage of variations in the polarization direction between ferroelectric domains [188] has been used, for example, to deposit patterns of silver lines with submicron dimensions [189]. Taking advantage of polarization direction variations at domain walls could lead to nanometric patterning, but it first requires a deep understanding of the variations of the band structure close to domain walls. Such information could be provided by photoluminescence microscopy measurements.

8.4. Conclusions

We believe that optical methods still have a great potential to understand structure and properties of domain walls. In spite of their limited spatial resolution, their sensitivity in general does give access to the physical mechanisms. They appear in fact essential to study domain walls as 3D objects, and in that sense are very complementary to the surface sensitivity of atomic force microscopy techniques, and to the very local information provided by electron microscopy. Technical improvements can be anticipated at several levels, with the development of super-resolved techniques, or advances in statistical data treatment for the extraction of specific signals. We hope that this review will inspire further studies of the kind, and contribute to progress in the exciting field of domain wall engineering.

Acknowledgment

ORCID iDs

G F Nataf https://orcid.org/0000-0001-9215-4717
M Guennou https://orcid.org/0000-0001-9349-3024

References

[1] Lawless W N and Fousek J 1970 *J. Phys. Soc. Japan* **28** 419–24
[2] Janovec V, Richterová L and Přívratská J 1999 *Ferroelectrics* **222** 73–6
[3] Aird A and Salje E K H 1998 *J. Phys.: Condens. Matter* **10** L377–80
[4] Salje E K H 2010 *ChemPhysChem* **11** 940–50
[5] Catalan G, Seidel J, Ramesh R and Scott J F 2012 *Rev. Mod. Phys.* **84** 119–56
[6] Seidel J 2012 *J. Phys. Chem. Lett.* **3** 2905–9
[7] Meier D 2015 *J. Phys.: Condens. Matter* **27** 463003
[8] Seidel J *et al* 2009 *Nat. Mater.* **8** 229–34
[9] Seidel J *et al* 2010 *Phys. Rev. Lett.* **105** 197603
[10] Guyonnet J, Gaponenko I, Gariglio S and Paruch P 2011 *Adv. Mater.* **23** 5377–82
[11] Farokhipoor S and Noheda B 2011 *Phys. Rev. Lett.* **107** 127601
[12] Meier D, Seidel J, Cano A, Delaney K, Kumagai Y, Mostovoy M, Spaldin N A, Ramesh R and Fiebig M 2012 *Nat. Mater.* **11** 284–8
[13] Rojac T *et al* 2016 *Nat. Mater.* **16** 322–7
[14] Ma J *et al* 2018 *Nat. Nanotechnol.* **13** 947–52
[15] Sluka T, Tagantsev A K, Bednyakov P and Setter N 2013 *Nat. Commun.* **4** 1808
[16] Goncalves-Ferreira L, Redfern S A T, Artacho E and Salje E K H 2008 *Phys. Rev. Lett.* **101** 097602
[17] Scott J F, Salje E K H and Carpenter M A 2012 *Phys. Rev. Lett.* **109** 187601
[18] Salje E K H, Aktas O, Carpenter M A, Laguta V V and Scott J F 2013 *Phys. Rev. Lett.* **111** 247603
[19] Wei X K, Tagantsev A K, Kvasov A, Roleder K, Jia C L and Setter N 2014 *Nat. Commun.* **5** 3031
[20] Yokota H, Usami H, Haumont R, Hicher P, Kaneshiro J, Salje E K H and Uesu Y 2014 *Phys. Rev. B* **89** 144109
[21] Yokota H, Niki S, Haumont R, Hicher P and Uesu Y 2017 *AIP Adv.* **7** 085315

[22] Yokota H, Matsumoto S, Salje E K H and Uesu Y 2018 *Phys. Rev. B* **98** 104105
[23] Yokota H, Matsumoto S, Salje E K H and Uesu Y 2019 *Phys. Rev. B* **100** 024101
[24] Nataf G F *et al* 2017 *Phys. Rev. Mater.* **1** 074410
[25] Van Aert S, Turner S, Delville R, Schryvers D, Van Tendeloo G and Salje E K H 2012 *Adv. Mater.* **24** 523–7
[26] Wei X K, Jia C L, Sluka T, Wang B X, Ye Z G and Setter N 2016 *Nat. Commun.* **7** 12385
[27] Gonnissen J, Batuk D, Nataf G F, Jones L, Abakumov A M, Van Aert S, Schryvers D and Salje E K H 2016 *Adv. Funct. Mater.* **26** 7599–604
[28] Schröder M, Haußmann A, Thiessen A, Soergel E, Woike T and Eng L M 2012 *Adv. Funct. Mater.* **22** 3936–44
[29] Schröder M, Chen X, Haußmann A, Thiessen A, Poppe J, Bonnell D A and Eng L M 2014 *Mater. Res. Express* **1** 035012
[30] Yang M M, Bhatnagar A, Luo Z D and Alexe M 2017 *Sci. Rep.* **7** 43070
[31] Hadni A, Henninger Y, Thomas R, Vergnat P and Wyncke B 1965 *J. Physique* **26** 345–60
[32] Hadni A and Thomas R 1972 *Ferroelectrics* **4** 39–49
[33] Hadni A and Thomas R 1974 *Ferroelectrics* **7** 177
[34] Hadni A and Thomas R 1975 *Phys. Status Solidi* a **31** 71–81
[35] Hadni A, Bassia J M, Gerbaux X and Thomas R 1976 *Appl. Opt.* **15** 2150
[36] Royer D, Dieulesaint E and Kummer P 1984 *Electron. Lett.* **20** 583
[37] Bierlein J D and Ahmed F 1987 *Appl. Phys. Lett.* **51** 1322–4
[38] Pradhan M and Garg R 1977 *Opt. Commun.* **20** 422–5
[39] Clay W, Evans B J and Latham R V 1974 *J. Phys. D: Appl. Phys.* **7** 316
[40] Latham R V 1976 *J. Phys. D: Appl. Phys.* **9** 2295–304
[41] Bhattacharyya A, Tuli S and Kataria S 1994 *IEEE Trans. Instrum. Meas.* **43** 30–3
[42] Batagiannis A, Wübbenhorst M and Hulliger J 2010 *Curr. Opi. Solid State Mater. Sci.* **14** 107–15
[43] McCord J 2015 *J. Phys. D: Appl. Phys.* **48** 333001
[44] Forsbergh P W 1949 *Phys. Rev.* **76** 1187–201
[45] Koralewski M and Szafrański M 1989 *Ferroelectrics* **97** 233–45
[46] Shur V Y, Gruverman A L, Letuchev V V, Rumyantsev E L and Subbotin A L 1989 *Ferroelectrics* **98** 29–49
[47] Rabe H, Rivera J P, Schmid H, Chaminade J P and Nganga L 1990 *Mater. Sci. Eng. B* **5** 243–8
[48] Dolino G 1975 *Rev. Phys. Appl.* **10** 433–6
[49] Merz W J 1952 *Phys. Rev.* **88** 421–2
[50] Müller M, Soergel E and Buse K 2003 *Opt. Lett.* **28** 2515
[51] Merz W J 1954 *Phys. Rev.* **95** 690–8
[52] Merz W J 1956 *J. Appl. Phys.* **27** 938–43
[53] Miller R C 1958 *Phys. Rev.* **111** 736–9
[54] Miller R C and Savage A 1959 *Phys. Rev. Lett.* **2** 294–6
[55] Miller R C and Savage A 1961 *J. Appl. Phys.* **32** 714–21
[56] Kobayashi J, Yamada N and Nakamura T 1963 *Phys. Rev. Lett.* **11** 410–4
[57] Březina B and Fotčenkov A A 1964 *Czech. J. Phys.* **14** 21–5
[58] Fousek J and Březina B 1960 *Czech. J. Phys.* **10** 511–28
[59] Fousek J and Březina B 1961 *Czech. J. Phys.* **11** 344–59
[60] Little E A 1955 *Phys. Rev.* **98** 978–84
[61] Pesquera D, Casals B, Thompson J E, Nataf G F, Moya X and Carpenter M A 2019 *APL Mater.* **7** 051109
[62] Aizu K 1973 *J. Phys. Soc. Japan* **34** 121–8
[63] Muñoz-Saldaña J, Schneider G A and Eng L M 2001 *Surf. Sci.* **480** L402–10
[64] Bloss F D 1961 *An Introduction to the Methods of Optical Crystallography* (New York: Saunders College Publishing)
[65] Wahlstrom E E 1979 *Opt. Crystallogr.* (New York: Wiley) p 489
[66] Schmid H 1993 *Ferroelectric Ceramics* ed N Setter and E L Colla (Basel: Birkhäuser) pp 107–26
[67] Soergel E 2005 *Appl. Phys. B* **81** 729–51
[68] Lang S B and Chan H L W 2007 *Frontiers of Ferroelectricity* (Boston, MA: Springer)
[69] Tagantsev A K, Cross L E and Fousek J 2010 *Domains in Ferroic Crystals and Thin Films* (New York: Springer)
[70] Glazer A M, Lewis J G and Kaminsky W 1996 *Proc. R. Soc. A* **452** 2751–65
[71] Shepherd I and Barkley J 1972 *Solid State Commun.* **10** 123–6
[72] Tsukamoto T, Hatano J and Futama H 1982 *J. Phys. Soc. Japan* **51** 3948–52
[73] Tsukamoto T, Hatano J and Futama H 1984 *J. Phys. Soc. Japan* **53** 838–43
[74] Tsukamoto T and Futama H 1993 *Phase Trans.* **45** 59–76
[75] Bednyakov P S, Sluka T, Tagantsev A K, Damjanovic D and Setter N 2015 *Sci. Rep.* **5** 15819
[76] Dougherty J P, Sawaguchi E and Cross L E 1972 *Appl. Phys. Lett.* **20** 364–5
[77] Pique J, Dolino G and Vallade M 1977 *J. Physique* **38** 1527–33
[78] Otko A I, Nosenko A E, Volk T R and Shuvalov L A 1993 *Ferroelectrics* **145** 163–80
[79] Gopalan V, Jia Q X and Mitchell T E 1999 *Appl. Phys. Lett.* **75** 2482–4
[80] Gopalan V and Mitchell T E 1999 *J. Appl. Phys.* **85** 2304–11
[81] Gopalan V, Gerstl S S A, Itagi A, Mitchell T E, Jia Q X, Schlesinger T E and Stancil D D 1999 *J. Appl. Phys.* **86** 1638–46
[82] Gopalan V and Gupta M C 1996 *J. Appl. Phys.* **80** 6099
[83] Tikhomirov O and Red'kin B 1999 *Ferroelectrics* **222** 339–43
[84] Otko A I, Krainyuk G G, Poplavko Y M and Shuvalov L A 1994 *Ferroelectr. Lett. Sect.* **18** 127–32
[85] Otko A I and Stasyuk I V 1995 *Ferroelectrics* **172** 207–15
[86] Otko A I, Nosenko A E, Gumennyi R M, Stasyuk I V and Solskii I M 1997 *Ferroelectrics* **191** 159–69
[87] Tikhomirov O, Red'kin B, Trivelli A and Levy J 2000 *J. Appl. Phys.* **87** 1932–6
[88] Tikhomirov O and Levy J 2003 *Ferroelectrics* **292** 161–9
[89] Wengler M, Buse K, Muller M and Soergel E 2004 *Appl. Phys. B* **78** 367–70
[90] Müller M, Soergel E, Buse K, Langrock C and Fejer M M 2005 *J. Appl. Phys.* **97** 044102
[91] Kösters M, Hartwig U, Woike T, Buse K and Sturman B 2006 *Appl. Phys. Lett.* **88** 182910
[92] Huang D *et al* 1991 *Science* **254** 1178–81
[93] Haußmann A, Kirsten L, Schmidt S, Cimalla P, Wehmeier L, Koch E and Eng L M 2017 *Ann. Phys., Lpz.* **1700139** 1700139
[94] Pei S C, Ho T S, Tsai C C, Chen T H, Ho Y, Huang P L, Kung A H and Huang S L 2011 *Opt. Express* **19** 7153
[95] Kirsten L, Haußmann A, Schnabel C, Schmidt S, Cimalla P, Eng L M and Koch E 2017 *Opt. Express* **25** 14871
[96] Gopalan V, Dierolf V and Scrymgeour D A 2007 *Annu. Rev. Mater. Res.* **37** 449–89
[97] Onuki K, Uchida N and Saku T 1972 *J. Opt. Soc. Am.* **62** 1030
[98] Nelson D F and Mikulyak R M 1974 *J. Appl. Phys.* **45** 3688–9
[99] Boyd R 2008 *Nonlinear Optics* (Amsterdam: Elsevier) p 640
[100] Hlinka J, Stepkova V, Marton P, Rychetsky I, Janovec V and Ondrejkovic P 2011 *Phase Trans.* **84** 738–46
[101] Rosenfeldt A and Flörsheimer M 2001 *Appl. Phys. B* **73** 523–9
[102] Maglione M, Theerthan A, Rodriguez V, Peña A, Canalias C, Ménaert B and Boulanger B 2016 *Opt. Mater. Express* **6** 137
[103] Kaneshiro J, Uesu Y and Fukui T 2010 *J. Opt. Soc. Am. B* **27** 888
[104] Fiebig M, Fröhlich D, Lottermoser T and Maat M 2002 *Phys. Rev. B* **66** 144102
[105] Fragemann A, Pasiskvicius V and Laurell F 2004 *Appl. Phys. Lett.* **85** 375–7

[106] Cherifi-Hertel S, Bulou H, Hertel R, Taupier G, Dorkenoo K D, Andreas C, Guyonnet J, Gaponenko I, Gallo K and Paruch P 2017 *Nat. Commun.* **8** 15768

[107] Uesu Y, Yokota H, Kawado S, Kaneshiro J, Kurimura S and Kato N 2007 *Appl. Phys. Lett.* **91** 182904

[108] Bozhevolnyi S I, Pedersen K, Skettrup T, Zhang X and Belmonte M 1998 *Opt. Commun.* **152** 221–4

[109] Bozhevolnyi S I, Hvam J M, Pedersen K, Laurell F, Karlsson H, Skettrup T and Belmonte M 1998 *Appl. Phys. Lett.* **73** 1814–6

[110] Flörsheimer M, Paschotta R, Kubitscheck U, Brillert C, Hofmann D, Heuer L, Schreiber G, Verbeek C, Sohler W and Fuchs H 1998 *Appl. Phys.* B **67** 593–9

[111] Sheng Y, Best A, Butt H J, Krolikowski W, Arie A and Koynov K 2010 *Opt. Express* **18** 16539

[112] Kämpfe T, Reichenbach P, Schröder M, Haußmann A, Eng L M, Woike T and Soergel E 2014 *Phys. Rev.* B **89** 035314

[113] Kämpfe T, Reichenbach P, Haußmann A, Woike T, Soergel E and Eng L M 2015 *Appl. Phys. Lett.* **107** 152905

[114] Godau C, Kämpfe T, Thiessen A, Eng L M and Haußmann A 2017 *ACS Nano* **11** 4816–24

[115] Dolino G 1973 *Appl. Phys. Lett.* **22** 123–4

[116] Liu B, Zheng Y, Zhao X, Liu H and Chen X 2016 *Opt. Express* **24** 29459

[117] Loudon R 1964 *Adv. Phys.* **13** 423–82

[118] Kong Y *et al* 2004 *Opt. Mater.* **27** 471–3

[119] Capek P, Stone G, Dierolf V, Althouse C and Gopolan V 2007 *Phys. Status Solidi* c **4** 830–3

[120] Stone G, Lee D, Xu H, Phillpot S R and Dierolf V 2013 *Appl. Phys. Lett.* **102** 042905

[121] Hammoum R, Fontana M D, Bourson P and Shur V 2007 *Appl. Phys.* A **91** 65–7

[122] Fontana M D, Hammoum R, Bourson P, Margueron S and Shur V Y 2008 *Ferroelectrics* **373** 26–31

[123] Zelenovskiy P S, Fontana M, Shur V, Bourson P and Kuznetsov D K 2010 *Appl. Phys.* A **99** 741–4

[124] Zelenovskiy P S, Shur V Y, Bourson P, Fontana M D, Kuznetsov D K and Mingaliev E A 2010 *Ferroelectrics* **398** 34–41

[125] Stone G and Dierolf V 2012 *Opt. Lett.* **37** 1032

[126] Nataf G F, Guennou M, Haußmann A, Barrett N and Kreisel J 2016 *Phys. Status Solidi RRL* **10** 222–6

[127] Nataf G F, Barrett N, Kreisel J and Guennou M 2018 *J. Phys.: Condens. Matter* **30** 035902

[128] Bismayer U, Mathes D, Aroyo M, Bosbach D, Putnis A, Van Tendeloo G and Güttler B 2000 *Phase Trans.* **71** 243–70

[129] Mihailova B, Bismayer U, Engelhardt A and Güttler B 2001 *J. Phys.: Condens. Matter* **13** 9383–92

[130] Rubio-Marcos F, Del Campo A, Marchet P and Fernández J F 2015 *Nat. Commun.* **6** 6594

[131] Everall N J 2000 *Appl. Spectrosc.* **54** 773–82

[132] Everall N J 2000 *Appl. Spectrosc.* **54** 1515–20

[133] Vij D 1998 *Luminescence of Solids* ed D R Vij (Boston, MA: Springer) (https://doi.org/10.1007/978-1-4615-5361-8)

[134] Dierolf V and Sandmann C 2007 *J. Lumin.* **125** 67–79

[135] Dierolf V and Koerdt M 2000 *Phys. Rev.* B **61** 8043–52

[136] Dierolf V, Sandmann C, Kim S, Gopalan V and Polgar K 2003 *J. Appl. Phys.* **93** 2295

[137] Dierolf V and Sandmann C 2004 *Appl. Phys.* B **78** 363–6

[138] Balsamo S, Maio S, Montrosset I, Suche H and Sohler W 1999 *Opt. Quantum Electron.* **31** 29–33

[139] Harris J, Norris G and McConnell G 2008 *Opt. Express* **16** 5667

[140] Reichenbach P, Kämpfe T, Thiessen A, Schröder M, Haussmann A, Woike T and Eng L M 2014 *J. Appl. Phys.* **115** 213509

[141] Reichenbach P, Kämpfe T, Thiessen A, Haußmann A, Woike T and Eng L M 2014 *Appl. Phys. Lett.* **105** 122906

[142] Yang T J, Mohideen U and Gupta M C 1997 *Appl. Phys. Lett.* **71** 1960–2

[143] Eng L M and Güntherodt H J 2000 *Ferroelectrics* **236** 35–46

[144] Tikhomirov O, Labardi M, Ascoli C and Allegrini M 2011 *J. Appl. Phys.* **110** 084117

[145] Canet-Ferrer J, Martín-Carrón L, Martínez-Pastor J, Valdes J L, Peña A, Carvajal J J and Diaz F 2007 *J. Microsc.* **226** 133–9

[146] Lifante G, Lamela J, Cantelar E, Jaque D, Cussó F, Zhu S N and Jaque F 2008 *Ferroelectrics* **363** 187–98

[147] Han T P J, Jaque F, Lamela J, Jaque D, Lifante G, Cusso F and Kamiskii A A 2009 *J. Phys.: Condens. Matter* **21** 042201

[148] Kim S and Gopalan V 2005 *Mater. Sci. Eng.* B **120** 91–4

[149] Camarillo E, Han T P J, Lamela J, García-Cabañes A, Carrascosa M, Lifante G and Jaque F 2014 *Ferroelectrics* **467** 6–12

[150] Yang T and Mohideen U 1998 *Phys. Lett.* A **250** 205–10

[151] Yang T, Gopalan V, Swart P and Mohideen U 2000 *J. Phys. Chem. Solids* **61** 275–82

[152] Lamela J, Ródenas A, Lifante G, Jaque D, Jaque F and Kaminskii A A 2008 *Laser Phys. Lett.* **5** 291–5

[153] García N, Levanyuk A P, Massanell J, Przeslawski J, Zlatkin A and Costa J L 1996 *Ferroelectrics* **184** 1–10

[154] Eng L M, Schlaphof F, Trogisch S, Roelofs A and Waser R 2001 *Ferroelectrics* **251** 11–20

[155] Stöckle R M, Suh Y D, Deckert V and Zenobi R 2000 *Chem. Phys. Lett.* **318** 131–6

[156] Berweger S and Raschke M B 2009 *J. Raman Spectrosc.* **40** 1413–9

[157] Berweger S, Neacsu C C, Mao Y, Zhou H, Wong S S and Raschke M B 2009 *Nat. Nanotechnol.* **4** 496–9

[158] Deckert-Gaudig T, Taguchi A, Kawata S and Deckert V 2017 *Chem. Soc. Rev.* **46** 4077–110

[159] Kaupp G 2006 *Atomic Force Microscopy, Scanning Nearfield Optical Microscopy and Nanoscratching* (Berlin: Springer) (https://doi.org/10.1007/978-3-540-28472-7)

[160] Lamela J, Jaque F, Cantelar E, Jaque D, Kaminskii A A and Lifante G 2007 *Opt. Quantum Electron.* **39** 805–11

[161] Meyer C, Hühn S, Jungbauer M, Merten S, Damaschke B, Samwer K and Moshnyaga V 2017 *J. Raman Spectrosc.* **48** 46–52

[162] Smith K A *et al* 2019 *Nat. Commun.* **10** 5235

[163] Janovec V and Přívratská J 2013 Domain structures *International Tables for Crystallography* vol D (Dordrecht: Springer) pp 484–543

[164] Warwick A R, Íñiguez J, Haynes P D and Bristowe N C 2019 *J. Phys. Chem. Lett.* **10** 1416–21

[165] Tolédano P, Guennou M and Kreisel J 2014 *Phys. Rev.* B **89** 134104

[166] Schranz W, Rychetsky I and Hlinka J 2019 *Phys. Rev.* B **100** 184105

[167] Tagantsev A K, Courtens E and Arzel L 2001 *Phys. Rev.* B **64** 224107

[168] Lee D, Behera R K, Wu P, Xu H, Li Y L, Sinnott S B, Phillpot S R, Chen L Q and Gopalan V 2009 *Phys. Rev.* B **80** 060102

[169] Lee D, Xu H, Dierolf V, Gopalan V and Phillpot S R 2010 *Phys. Rev.* B **82** 014104

[170] Behera R K, Lee C W, Lee D, Morozovska A N, Sinnott S B, Asthagiri A, Gopalan V and Phillpot S R 2011 *J. Phys.: Condens. Matter* **23** 175902

[171] Stepkova V, Marton P and Hlinka J 2012 *J. Phys.: Condens. Matter* **24** 212201

[172] Taherinejad M, Vanderbilt D, Marton P, Stepkova V and Hlinka J 2012 *Phys. Rev.* B **86** 155138

[173] Eliseev E A, Morozovska A N, Gu Y, Borisevich A Y, Chen L Q, Gopalan V and Kalinin S V 2012 *Phys. Rev.* B **86** 085416

[174] Eliseev E, Yudin P, Kalinin S, Setter N, Tagantsev A and Morozovska A 2013 *Phys. Rev.* B **87** 054111

[175] Jia C L, Mi S B, Urban K, Vrejoiu I, Alexe M and Hesse D 2008 *Nat. Mater.* **7** 57–61

[176] Li L, Gao P, Nelson C T, Jokisaari J R, Zhang Y, Kim S J, Melville A, Adamo C, Schlom D G and Pan X 2013 *Nano Lett.* **13** 5218–23

[177] Ding X and Salje E K H 2015 *AIP Adv.* **5** 053604

[178] Li S, Ding X, Ren J, Moya X, Li J, Sun J and Salje E K H 2015 *Sci. Rep.* **4** 6375

[179] Liu C, Chen Y and Dames C 2019 *Phys. Rev. Appl.* **11** 044002

[180] Seijas-Bellido J A, Escorihuela-Sayalero C, Royo M, Ljungberg M P, Wojdeł J C, Íñiguez J and Rurali R 2017 *Phys. Rev.* B **96** 140101

[181] Royo M, Escorihuela-Sayalero C, Íñiguez J and Rurali R 2017 *Phys. Rev. Mater.* **1** 051402

[182] Mante A and Volger J 1971 *Physica* **52** 577–604

[183] Weilert M A, Msall M E, Wolfe J P and Anderson A C 1993 *Z. Phys.* B **91** 179–88

[184] Liu Y, Dkhil B and Defay E 2016 *ACS Energy Lett.* **1** 521–8

[185] Yang S Y *et al* 2010 *Nat. Nanotechnol.* **5** 143–7

[186] Bhatnagar A, Roy Chaudhuri A, Heon Kim Y, Hesse D and Alexe M 2013 *Nat. Commun.* **4** 2835

[187] Weber M C, Guennou M, Toulouse C, Cazayous M, Gillet Y, Gonze X and Kreisel J 2016 *Phys. Rev.* B **93** 125204

[188] Li L, Salvador P A and Rohrer G S 2014 *Nanoscale* **6** 24–42

[189] Giocondi J L and Rohrer G S 2001 *Chem. Mater.* **13** 241–2